catalysts

MDPI

Article

Phase Transformation of Zr-Modified $LaNiO_3$ Perovskite Materials: Effect of CO_2 Reforming of Methane to Syngas

Tatiparthi Vikram Sagar [1,2,*], Nakka Lingaiah [2], Potharaju S. Sai Prasad [2], Nataša Novak Tušar [3] and Urška Lavrenčič Štangar [1,*]

[1] Faculty of Chemistry and Chemical Technology, University of Ljubljana, Večna Pot 113, 1000 Ljubljana, Slovenia
[2] Department of Catalysis and Fine Chemicals, CSIR-Indian Institute of Chemical Technology, Hyderabad 500007, India
[3] Department of Inorganic Chemistry and Technology, National Institute of Chemistry, Hajdrihova 19, 1001 Ljubljana, Slovenia
* Correspondence: vikram.sagartatiparthi@fkkt.uni-lj.si (T.V.S.); urska.lavrencic.stangar@fkkt.uni-lj.si (U.L.Š.); Tel.: +386-14798675 (U.L.Š.)

Abstract: Zr-modified $LaNiO_3$ catalysts ($LaNi_xZr_{1-x}O_3$; $0 \leq x \leq 1$) are synthesized by the sol–gel method. The physio-chemical properties of materials are investigated using different characterization techniques and evaluated for the CO_2 reforming of methane to syngas. Interestingly, the characterization studies revealed the phase transformation from La-Zr pyrochlore to La-Ni perovskite depending on the Ni:Zr ratio in the material. The formation of the pyrochlore phase is observed for high-Zr-containing catalysts, thus leading to the production of bulk NiO. The formation of La-Ni perovskite is observed for high-Ni-containing catalysts and the ZrO_2 acted as a support. The formation of La-Ni perovskite supported on ZrO_2 enhanced the Ni dispersion of the catalysts. The high dispersion of Ni enhanced the catalytic activity, and $LaNi_{0.8}Zr_{0.2}O_3$ showed the best performance among all of the studied catalysts in terms of conversions and the H_2/CO ratio.

Keywords: $LaNiO_3$ perovskite; syngas; hydrogen; CO_2 reforming; La-Zr pyrochlore

check for updates

Citation: Sagar, T.V.; Lingaiah, N.; Sai Prasad, P.S.; Tušar, N.N.; Štangar, U.L. Phase Transformation of Zr-Modified $LaNiO_3$ Perovskite Materials: Effect of CO_2 Reforming of Methane to Syngas. *Catalysts* **2024**, *14*, 91. https://doi.org/10.3390/catal14010091

Academic Editors: Mingjun Jia and Xintong Zhang

Received: 29 December 2023
Revised: 19 January 2024
Accepted: 19 January 2024
Published: 22 January 2024

Copyright: © 2024 by the authors. Licensee MDPI, Basel, Switzerland. This article is an open access article distributed under the terms and conditions of the Creative Commons Attribution (CC BY) license (https://creativecommons.org/licenses/by/4.0/).

1. Introduction

The dry reforming of methane (DRM) is a process that converts potent greenhouse gases (CH_4 and CO_2) into useful syngas (H_2/CO ratio = 1) [1,2]. The syngas has many advantages; one of the main advantages is that it can be used as a feedstock for Fischer–Tropsch synthesis to produce a higher number of hydrocarbons and produce oxygenated derivatives. As the DRM reaction operates at 600–800 °C, the catalyst suffers from sintering and coking. So, designing a catalyst for the high-temperature reaction is a difficult task [3].

The applications of Ni-based structured oxides as catalysts for the reaction are many, and the active metal can be isomorphically substituted into various structures to enhance the catalytic activity [1]. The active metal in these materials is bound within the structure, thereby increasing the thermal stability towards the sintering of active particles. The oxygen mobility in the catalyst can be enhanced by the substitution of active metals into the lattice, which helps to enhance the resistance towards carbon deposition [4–6]. The structural materials tested to date include perovskite, pyrochlore, fluorite, and hexaaluminate [6–10]. Pyrochlores are highly crystalline mixed metal oxides, having the general formula $A_2B_2O_7$. The A-site of these materials is usually occupied by the large rare-earth trivalent metal such as La, and the B-site is occupied by a smaller tetravalent transition metal such as Zr. Several La- and Zr-based catalysts were studied [11–15]. However, the $Eu_2Ir_2O_7$ pyrochlore materials were first used to study the DRM reaction by Ashcroft et al. [16–18].

In this article, studies on Zr-modified $LaNiO_3$ catalysts ($LaNi_xZr_{1-x}O_3$) with varying x values synthesized by the sol–gel method are presented. The structural properties of

the catalysts are analyzed with nitrogen sorption (BET method), powder X-ray diffraction (XRD), temperature-programmed reduction (TPR), Fourier transform infrared spectroscopy (FT–IR), X-ray photoelectron spectroscopy (XPS), and CHNS (carbon analysis in used catalysts) techniques. The synthesized catalysts are evaluated for the DRM reaction. The transformation from a perovskite structure to pyrochlore structure with the addition of Zr into the $LaNiO_3$ oxide framework and its influence on the catalytic performance of the material towards syngas production by the DRM reaction are presented.

2. Results and Discussion

2.1. X-ray Diffraction Studies

XRD patterns of $LaNi_xZr_{1-x}O_3$ catalysts synthesized by the sol–gel method are reported in Figure 1. With the change in Ni content, a variety of solid phases appeared in the catalysts. Low-Ni–containing catalysts exhibited high intense diffraction peaks at 2θ = 28, 31, 47, and 55°. These peaks correspond to the compound of the general formula $La_2Zr_2O_7$, having a crystalline cubic structure of a typical pyrochlore compound (JCPDS 01-073-0444). Along with this, a low-intensity $LaNiO_3$ perovskite phase (JCPDS 34–1181) formation was also observed. On the other hand, the catalyst with high Ni loading (x = 0.8) showed a completely different trend by the formation of the $LaNiO_3$ bimetallic rhombohedral perovskite phase (JCPDS 34–1181). A low-intensity peak was observed at 2θ = 43° in all the catalysts synthesized, which is ascribed to NiO (JCPDS 78–0643). With the increase in Ni content, the intensity of the perovskite peak increased, indicating the formation of a highly crystalline phase.

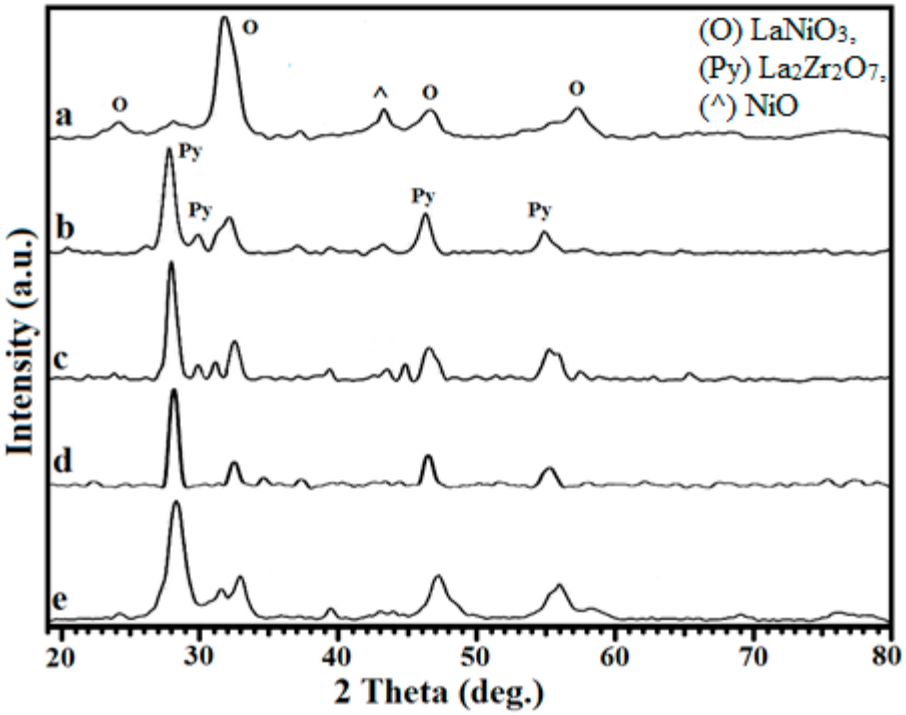

Figure 1. XRD patterns of $LaNi_xZr_{1-x}O_3$ catalysts synthesized by sol–gel method: (a) x = 0.8, (b) x = 0.6, (c) x = 0.4, (d) x = 0.3, and (e) x = 0.2.

A study conducted by Bespalko et al. [19] on Ni–La–Zr oxide catalysts prepared by the sol–gel method indicated the formation of $La_2Zr_2O_7$ along with NiO in a mono oxide phase. From their crystallographic studies, they concluded that the formation of the bimetallic pyrochlore phase proceeded due to the formation of the biphasic system (MeLaZr → MeOx + $La_2Zr_2O_7$) [19]. The same group (Bussi et al. [20]) opined that the amorphous oxide formed might be converted into a biphasic system (NiLaZr mixed oxides)$_{amorphous}$ → NiO + $La_2Zr_2O_7$) [20]. Studies carried out by Gaur et al. [21] on dop-

ing Rh, Ni, and Ca into La–Zr pyrochlore showed the formation of a discrete Ni oxide peak other than the pyrochlore structure in the case of Ca due to the incorporation of a Ca^{2+} cation in place of a La^{3+} cation. The oxygen vacancies led to structural defects and eventually to the formation of the $CaZrO_3$ perovskite phase. They also concluded that the low levels of substitution at the B–site did not have much of an effect on the pyrochlore structure [21].

According to the above studies, the formation of pyrochlore with La–Zr catalysts are more favorable in the low B–site modification. These findings are very much in agreement with the observations made in the present study, where the pyrochlore phase dominated in low-Ni-containing samples. On the other hand, with the increase in Ni loading, the formation of $LaNiO_3$ perovskite became more favorable than La–Zr pyrochlore. These typical phase changes were observed with changes in Ni content and these findings are in good agreement with the previous research.

2.2. Specific Surface Area Measurements

The specific surface areas of $LaNi_xZr_{1-x}O_3$ catalysts prepared by the sol–gel method were determined by the BET method and are reported in Table 1. Surface areas of $LaNi_xZr_{1-x}O_3$ catalysts decreased with an increase in the Ni content. This may be due to the pore blockage of the LaZr-pyrochlore with NiO. As described in our previous articles, the surface areas of the catalysts are dependent on the calcination temperature [22,23]. With the increase in Ni content, the surface area dropped to 3.39 m^2/g when x = 0.6 was reached. The small increase in surface area at x = 0.8 is seen due to the formation of $LaNiO_3$ perovskite on the ZrO_2 surface, as we observed in the XRD study.

Table 1. Specific surface areas of $LaNi_xZr_{1-x}O_3$ catalysts synthesized by sol–gel method.

S. No.	Catalysts	Specific Surface Area (m^2/g)
1	$LaNi_{0.2}Zr_{0.8}O_3$	14
2	$LaNi_{0.3}Zr_{0.7}O_3$	12
3	$LaNi_{0.4}Zr_{0.6}O_3$	7
4	$LaNi_{0.6}Zr_{0.4}O_3$	3
5	$LaNi_{0.8}Zr_{0.2}O_3$	5

2.3. Fourier Transform Infrared Spectroscopy Studies

FTIR spectra of $LaNi_xZr_{1-x}O_3$ oxide catalysts synthesized by the sol–gel method are presented in Figure 2. In catalysts with a low Ni content, the –O–H stretching band of the physisorbed inner-layer water species appeared at 3200–3500 cm^{-1}. The bands at 1072–1180 and 1472–1424 cm^{-1} correspond to Zr–O and O–C=O of the carboxylate spices in the metal propionates, respectively, which suggest that traces of propionates are still present after calcination. Studies on La–Zr-oxide thin films by Chen et al. [24] revealed that the FT–IR transmittance bands at 3200–3500, 1039–1125, and 1403–1541 cm^{-1} related to –O–H, Zr–O–C, and O–C=O species, respectively. In another study conducted by Koteswara Rao et al. [25], high-intensity bands of the $La_2Zr_2O_7$ pyrochlore phase were seen in the absorption region of 1120–1110 cm^{-1} due to the Zr–O vibrations.

According to Tong et al. [26], in La–Zr pyrochlore, the ZrO_6 vibrational mode is observed at 539 cm^{-1}. As Ni content increased, the intensities of the bands corresponding to Zr–O and ZrO_6 decreased and almost disappeared in higher-Ni-containing catalysts. When x = 0.8, all the other bands were minimized, and the peaks noticed were due to the metal–oxygen stretching frequencies. The FT–IR spectra recorded in the present study are in good agreement with the previous observations [24–26]. The finding from the FT–IR analysis is well corroborated with the results of X-ray diffraction studies.

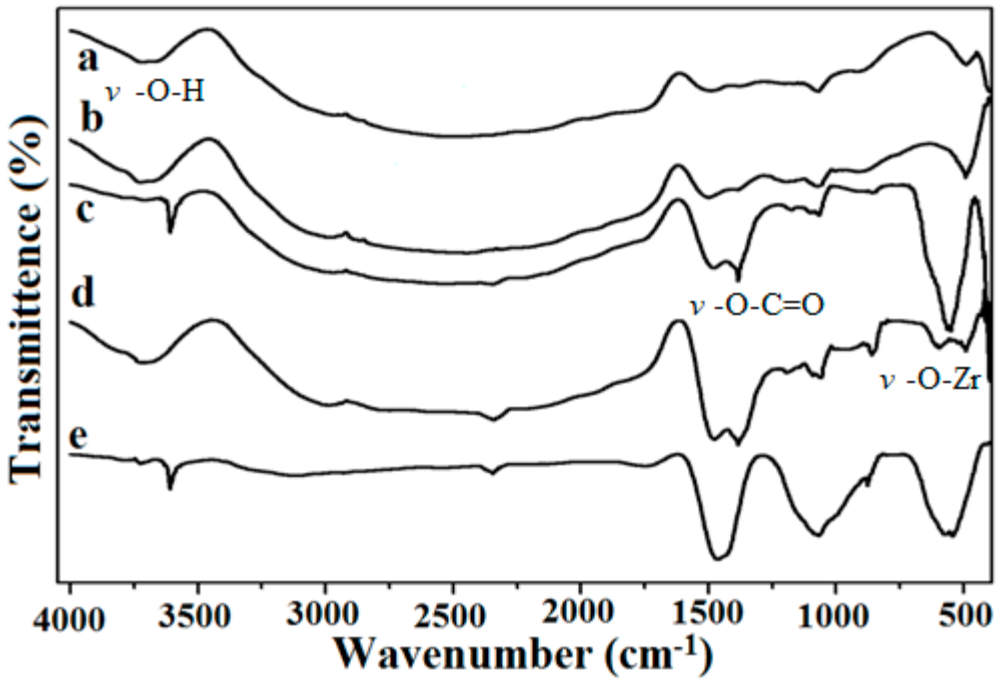

Figure 2. FT-IR patterns of $LaNi_xZr_{1-x}O_3$ catalysts synthesized by sol–gel method: (a) x = 0.8, (b) x = 0.6, (c) x = 0.4, (d) x = 0.3, and (e) x = 0.2.

2.4. Temperature-Programmed Reduction Studies

Reduction studies on $LaNi_xZr_{1-x}O_3$ catalysts have been carried out by varying the Ni content in the range of x = 0.2 to 0.8, and the results are depicted in Figure S1. The reduction peaks appeared in two zones, with the first falling in the temperature zone of 400–600 °C and the second falling in the temperature zone of > 600 °C. Bussi et al. [27], in their studies on Ni/LaZr pyrochlore catalysts, demonstrated the difference in the properties of Ni catalysts prepared by the co-precipitation and impregnation methods, particularly in the reduction behavior. The catalysts prepared by the co–precipitation method showed their reduction peaks at temperatures higher than 550 °C, implying a strong interaction of Ni with La–Zr pyrochlore. In contrast, in the catalysts prepared by the impregnation method, the major reduction peak appeared at T < 500 °C due to the NiO available on the surface of the La–Zr mixed oxide [27]. In the present investigation, the reduction patterns of $LaNi_xZr_{1-x}O_3$ catalysts prepared by the sol–gel method followed a similar trend. At low concentrations of Ni, it has a high interaction with supporting, La–Zr pyrochlore leading to the domination of a high-temperature peak. As the Ni content increases, the NiO exists in a highly dispersed state on La–Zr pyrochlore. Consequently, the reduction temperature decreased. The dispersed NiO is easily reduced, yielding Ni^0 species at lower temperatures.

2.5. X-ray Photoelectric Spectroscopy Studies

La 3d core-level XP spectra of $LaNi_xZr_{1-x}O_3$ catalysts synthesized by the sol–gel method are shown in Figure S2. The spectra showed two peaks corresponding to La $3d_{5/2}$ with binding energies at 834 and 838 eV, as observed in the studies presented in our previous articles. The splitting of the ~4 eV peak is due to the charge transfer from ligand (O 2p) to metal (La 4f). A similar observation was also made by Lima et al. [28] in their study on $La_xCe_{1-x}NiO_3$. In another study, Xu et al. [29] noticed the doublet peak for La $3d_{5/2}$ appearing at 834.3 and 838.2 eV. They concluded that these binding energy values are higher than the simple La_2O_3. Hence, they predicted the possibility of a La–Zr solid solution/pyrochlore formation [29]. In the present study, the binding energy peaks in the ranges of 834.3–838.5 and 851–852 eV correspond to $3d_{5/2}$ and $3d_{3/2}$, respectively [28]. These peaks confirm the presence of La^{3+} on the surface of the catalysts. The other peak at

851–852 eV is due to La $3d_{3/2}$. However, due to the overlapping of binding energies of La $3d_{3/2}$ and Ni $2p_{3/2}$, it is very difficult to interpret their peaks.

XP spectra of Ni 2p are presented in Figure 3. The nanoparticle NiO binding energy peaks are observed at 853–854 eV [21,30]. In the present study, the peaks with binding energies at 851 and 855 eV correspond to Ni $2p_{3/2}$. These binding energies of Ni are higher than the simple NiO, signifying that Ni is stabilized in a higher oxidation state, thus confirming the possible formation of perovskite in the catalyst samples with a high Ni content. The same observation was also made by Gaur et al. [21] in their studies on Rh, Ni, and Ca-substituted $La_2Zr_2O_7$ pyrochlore catalysts. They observed higher binding energies for Ni $2p_{3/2}$ than the regular NiO (Ni^{2+}). They attributed this high-binding energy shift to the existence of Ni in Ni_2O_3 (Ni^{3+}). Other studies conducted on perovskite-type oxide catalysts also showed higher binding energy peaks than regular NiO, indicating the presence of Ni^{3+} [28]. This is due to the high oxygen environment around Ni. With the increase in Ni content in the catalysts, the peak is shifted towards a higher binding energy value. This is also well corroborated with the results obtained from XRD studies which revealed that the formation of the perovskite phase is dominant in higher-Ni-containing samples.

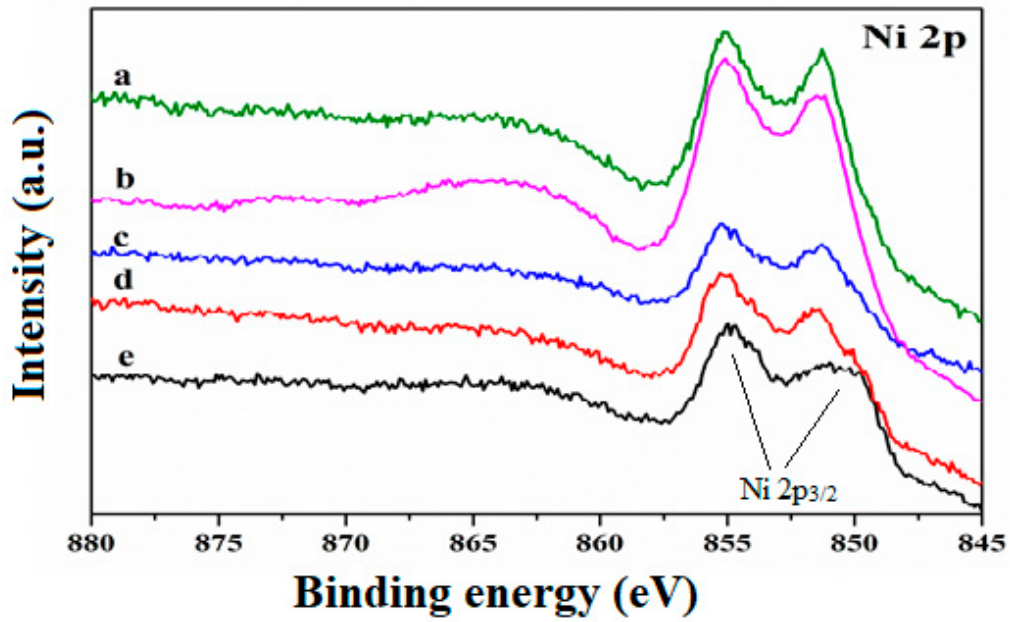

Figure 3. Ni 2p core-level spectra of $LaNi_xZr_{1-x}O_3$ catalysts synthesized by sol–gel method: (a) x = 0.8, (b) x = 0.6, (c) x = 0.4, (d) x = 0.3, and (e) x = 0.2.

Figure 4 shows the Zr 3d XP spectra of the $LaNi_xZr_{1-x}O_3$ catalysts synthesized by the sol–gel method. In the present study, the bands corresponding to Zr^{4+} in zirconium oxide appearing at 181.3 and 183.7 eV are attributed to Zr $3d_{5/2}$ and Zr $3d_{3/2}$, respectively [31,32]. However, in low-Ni-containing catalysts, the binding energy values recorded are a little lower, indicating that the Zr is in a lower oxidation state due to the structural defects arising from the strong interaction with other metals. With the increase in Ni content in the catalysts, the binding energy bands shifted to a higher value, indicating that the Zr is stabilized in ZrO_2. In the Zr 3d XP spectra reported by Xu et al. [29], the peaks corresponding to binding energies of 181.3 and 183.7 eV were of Zr $3d_{5/2}$ and Zr $3d_{3/2}$, respectively, with the splitting of binding energies being 2.4 eV. This photoemission feature is well corroborated with the previous literature [29].

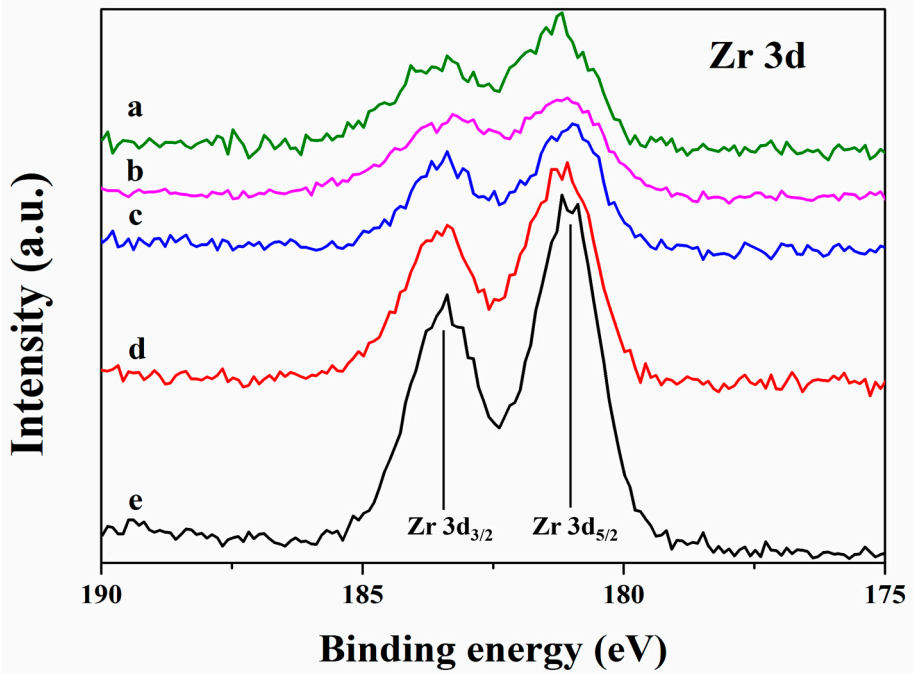

Figure 4. Zr 3d core-level spectra of $LaNi_xZr_{1-x}O_3$ catalysts synthesized by sol–gel method: (a) x = 0.8, (b) x = 0.6, (c) x = 0.4, (d) x = 0.3, and (e) x = 0.2.

The XPS O 1 s of all catalysts are provided in Figure 5(1). The broad peak of O 1 s is deconvoluted into triplet peaks at 528, 530, and 531 eV, as shown in Figure 5(2). These triplet peaks are ascribed to the M-O of the lattice oxygen (530 eV), M-O of the lattice vacancies (528 eV), and Zr-OH of the hydroxyl group (531 eV) on the surface [33,34].

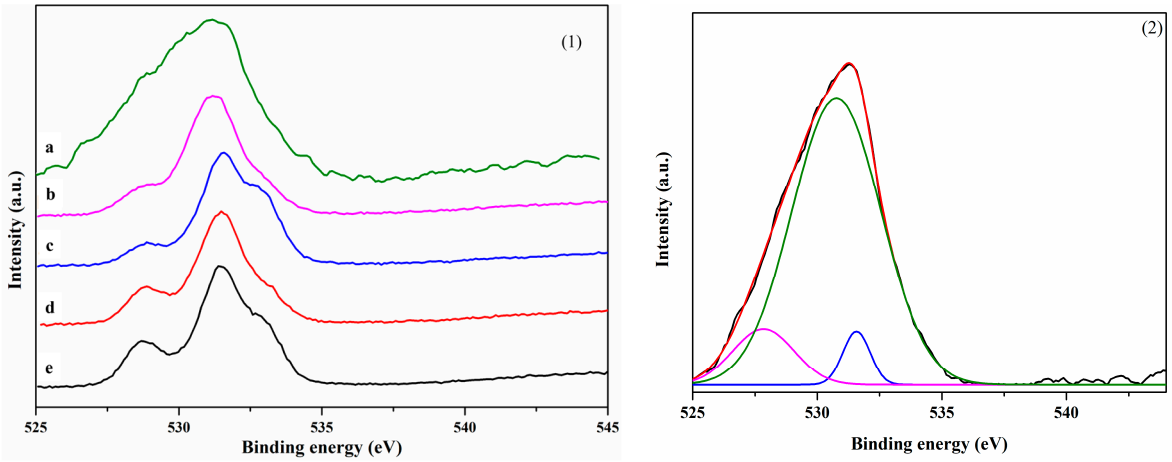

Figure 5. (**1**) O 1 s core-level spectra of $LaNi_xZr_{1-x}O_3$ catalysts synthesized by sol–gel method: (a) x = 0.8, (b) x = 0.6, (c) x = 0.4, (d) x = 0.3, and (e) x = 0.2; (**2**) deconvoluted O 1 s XPS of $LaNi_{0.8}Zr_{0.2}O_3$ catalyst.

2.6. Catalytic Activity

The DRM reaction was conducted over the synthesized $LaNi_xZr_{1-x}O_3$ catalysts using the feed in the ratio of CH_4:CO_2:N_2 = 80:80:80 and a total gas flow rate of 240 mL/min in a fixed-bed reactor. Figure 6 shows the activity profiles of $LaNi_xZr_{1-x}O_3$ oxide catalysts observed at 800 °C. The conversion of both methane and carbon dioxide progressively increased with an increase in the Ni content in the catalysts and attained their maximum values with catalysts having an x value of 0.8. The reducibility of the catalysts increased with the increase in Ni content. The catalytic activity also followed the same trend. As the

Ni ratio increased, the formation of dispersed Ni with La–Zr support increased, leading to enhanced activity. On the other hand, catalysts with a lower Ni ratio (x = 0.2–0.4) showed a greater interaction with the support, lowering the reducibility. Among the series, x = 0.8 catalysts showed the highest activity with a 50% CO_2 conversion and 37% CH_4 conversion along with a syngas ratio of 0.76. This trend of a higher conversion of CO_2 over methane was also identified by other researchers [28,35]. Bachiller-Baeza et al. [35] observed that the DRM reaction is always accompanied by side reactions like the reverse water–gas shift reaction (RWGS). This reaction consumes H_2 produced in the DRM reaction to form CO, thereby decreasing the syngas ratio.

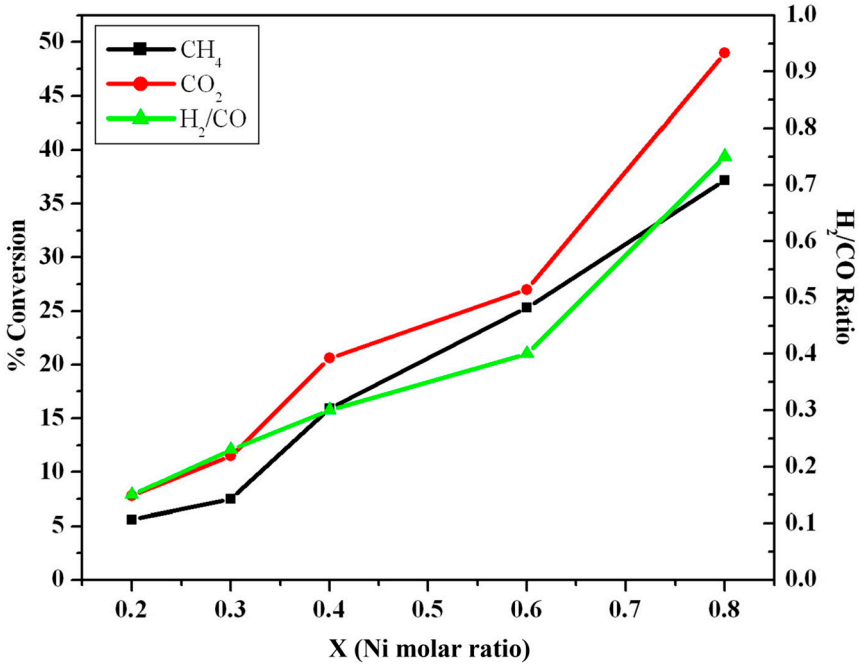

Figure 6. Catalytic activity study on DRM reaction over $LaNi_xZr_{1-x}O_3$ catalysts synthesized by sol–gel method (CH_4:CO_2:N_2 = 80:80:80; temperature = 800 °C).

In the XRD studies, the peaks due to free NiO were not observed clearly in low-Ni-containing catalysts, probably due to its amorphous nature. The increase in Ni content in the catalysts changed the nature of the phase from La–Zr pyrochlore to La–Ni perovskite. This phase transformation was also confirmed in the XPS studies. Catalysts with a higher Ni content after reduction could lead to the formation of Ni metal with its high dispersion on La_2O_3 and also free Ni in the bulk form. This may be the reason for the higher activity of the catalysts with a high Ni content.

Figure S3 shows the time-on-stream study of the $LaNi_{0.8}Zr_{0.2}O_3$ catalyst at 800 °C for 10 h for the DRM reaction. The catalyst showed reasonable stability for 10 h. There was no decrease in the percentage CH_4 conversion over the period of study (10 h), but after 4 h of reaction, the percentage CO_2 conversion started to decline and concurrently, the syngas ratio also decreased. The high initial conversion of CO_2 could be due to the RWGS reaction. It is known that RWGS reaction is favorable when carried out on La–Zr pyrochlore catalysts [35].

2.7. Carbon Analysis of the Used Catalysts

The amount of carbon formed on the $LaNi_xZr_{1-x}O_3$ catalysts was estimated after the DRM reaction and the data obtained are reported in Table S1. The catalysts with low Ni loading showed a high amount of carbon formation. Catalysts with high Ni content of $\geq$0.6, originally existing in the $LaNiO_3$ perovskite phase, tended to produce highly dispersed Ni on La_2O_3–ZrO_2 during the reduction and enhanced the coke resistance.

3. Experimental

3.1. Synthesis of Catalysts by Sol–Gel Method

$LaNi_xZr_{1-x}O_3$ are synthesized by sol–gel method with x values varying from 0 to 1 with a 0.2 step-wise increment. The calculated amounts of the respective nitrate salts (Lanthanum(III) nitrate, Nickel(II) nitrate, and Zirconyl(II) nitrate) necessary for each x value ($0 \leq x \leq 1$) were dissolved separately in hot propionic acid. The resulting propionate solutions were mixed and subjected to 30 min of vigorous stirring. The resulting solutions were treated for reflux for 24 h and then the obtained paste was dried under reduced pressure until the formation of the resin. The resulting solids were oven-dried and calcined at 800 °C, with a temperature ramp of 2 °C/min, and maintained at the same temperature for 4 h.

3.2. Characterization Studies

The crystal phases of the catalysts were obtained on an XRD instrument (Ultima-IV diffractometer, Rigaku Corporation, Tokyo, Japan) using Cu Kα radiation (λ = 1.54 Å). The measurements were recorded in the range of 10 to 80° with a step of 0.045°. The specific surface areas of the catalysts were determined by a SMART SORB 92/93 instrument. Before BET measurement, the samples were dried at 150 °C for 2 h. TPR studies were performed using a homemade apparatus with 50 mg of the catalyst loaded in a quartz reactor, and catalyst reduction was conducted with a 10% H_2-balanced Ar gas mixture flowing at a rate of 30 mL/min and with a heating rate of 5 °C/min up to 900 °C. The hydrogen consumption was monitored using a gas chromatograph (Varian, 8301). FT–IR spectra were obtained on a Perkin Elmer (Spectrum GX, MS, Waltham, MA, USA) instrument using the KBr pellet method. XPS measurements were made on a KRATOS AXIS 165 instrument. The coke content of the used catalysts was determined using a CHNS analyzer (ElementaV, Bad Friedrichshall, Germany).

3.3. Catalytic Activity

The evaluation of catalysts was performed in a fixed-bed Inconel reactor under atmospheric pressure by passing a mixture of CO_2, CH_4, and N_2 at a ratio of 80/80/80 (total flow rate = 240 mL/min and GHSV of 28,800 h^{-1}). Prior to the activity measurements, the samples were reduced in-situ under a 60% H_2-balanced N_2 gas mixture at 600 °C for 6 h. After attaining the required temperature, the reaction was allowed to attain a steady state for a period of 1 h. For each analysis, the gas products were analyzed two times with an interval of 30 min. The activity results provided in this study are the average values of two consecutive analyses. The product analysis was carried out online on a Nucon 5765 gas chromatograph equipped with a Carbosphere column using argon gas as a carrier with a TCD detector. The accuracy of the catalytic activity results is within the error margin of ±3%.

4. Conclusions

The results presented here deal with characterization and activity studies on $LaNi_xZr_{1-x}O_3$ catalysts synthesized by the sol–gel method. The effect of the Ni content on the performance of $LaNi_xZr_{1-x}O_3$ oxide catalysts ($0 < x < 1$) was studied for the dry reforming of methane reaction. At x = 0.2, the formation of the $La_2Zr_2O_7$ pyrochlore phase was observed. With the increase in Ni content, the pyrochlore phase disappeared at x = 0.8 and the $LaNiO_3$ perovskite oxide phase was formed. The catalyst with a high x value (x = 0.8) produced well-dispersed Ni metal species supported on La_2O_3 upon reduction. Among the series of $LaNi_xZr_{1-x}O_3$ catalysts studied, the catalyst with x = 0.8 showed the highest efficiency in terms of CH_4 and CO_2 conversions. It was observed that the formation of the perovskite phase plays a key role in the stability of the catalyst by controlling coke formation during the DRM reaction.

Supplementary Materials: The following supporting information can be downloaded at: https://www.mdpi.com/article/10.3390/catal14010091/s1, Figure S1: TPR Profiles of $LaNi_xZr_{1-x}O_3$ catalysts synthesized by sol-gel method. (a) x = 0.8, (b) x = 0.6, (c) x = 0.4, (d) x = 0.3, and (e) x = 0.2, Figure S2: La 3d Core level spectra of $LaNi_xZr_{1-x}O_3$ catalysts synthesized by sol-gel method. (a) x = 0.8, (b) x = 0.6, (c) x = 0.4, (d) x = 0.3 and (e) x = 0.2, Figure S3: Time on stream study of $LaNi_{0.8}Zr_{0.2}O_3$ catalysts synthesized by sol-gel method during DRM reaction at 800 °C, Table S1: Carbon formation during the DRM reaction on $LaNi_xZr_{1-x}O_3$ catalysts synthesized by sol-gel method.

Author Contributions: T.V.S.: Data curation; Formal analysis; Methodology; Investigation; Writing—original draft; N.L.: Validation; Writing—review & editing, P.S.S.P.: Supervision; Validation; Writing—review & editing, N.N.T.: Resources; Writing—review & editing and U.L.Š.: Writing—review & editing; Funding acquisition; Resources; Visualization. All authors have read and agreed to the published version of the manuscript.

Funding: The authors acknowledge the financial support from the Slovenian Research Agency (projects N2-0188, J2-4441) and through the core research funding (programs P1-0134 and P1-0418).

Data Availability Statement: Data sharing is not applicable to this article.

Acknowledgments: The authors acknowledge the financial support from the Slovenian Research Agency through the core research funding (programs J2-4441, N2-0188, P1-0134, and P1-0418). The COST action CA20126 (Network for research, innovation and product development on porous semiconductors and oxides, NETPORE) is also acknowledged.

Conflicts of Interest: The authors declare no conflicts of interest.

References

1. Pakhare, D.; Spivey, J. A review of dry (CO_2) reforming of methane over noble metal catalysts. *Chem. Soc. Rev.* **2014**, *43*, 7813–7837. [CrossRef] [PubMed]
2. Yan, Z.; Wang, Z.; Bukur, D.B.; Goodman, D.W. Fischer–Tropsch synthesis on a model Co/SiO_2 catalyst. *J. Catal.* **2009**, *268*, 196–200. [CrossRef]
3. Fidalgo, B.; Menéndez, J.A. Syngas production by CO_2 reforming of CH_4 under microwave heating-Challenges and opportunity. In *Syngas: Production, Applications and Environmental Impact*; Indarto., A., Palguandi., J., Eds.; Nova Science Publishers, Inc.: Hauppauge, NY, USA, 2013; pp. 121–149. ISBN 978-1-62100-870-5.
4. Mallikarjun, G.; Sagar, T.V.; Swapna, S.; Raju, N.; Chandrashekar, P.; Lingaiah, N. Hydrogen rich syngas production by bi-reforming of methane with CO_2 over Ni supported on CeO_2-SrO mixed oxide catalysts. *Catal. Today* **2020**, *356*, 597–603. [CrossRef]
5. Gardner, T.H.; Spivey, J.J.; Campos, A.; Hissam, J.C.; Kugler, E.L.; Roy, A.D. Catalytic partial oxidation of CH_4 over Ni-substituted barium hexaaluminate catalysts. *Catal. Today* **2010**, *157*, 166–169. [CrossRef]
6. Sagar, T.V.; Padmakar, D.; Lingaiah, N.; Reddy, I.A.K.; Sai Prasad, P.S. Syngas production by CO_2 reforming of methane on $LaNi_xAl_{1-x}O_3$ perovskite catalysts: Influence of method of preparation. *J. Chem. Sci.* **2017**, *129*, 1787–1794. [CrossRef]
7. Kumar, P.; Srivastava, V.C.; Štangar, U.L.; Mušič, B.; Mishra, I.M.; Meng, Y. Recent progress in dimethyl carbonate synthesis using different feedstock and techniques in the presence of heterogeneous catalysts. *Catal. Rev.* **2021**, *63*, 363–421. [CrossRef]
8. Nuvula, S.; Sagar, T.V.; Valluri, D.K.; Prasad, P.S. Selective substitution of Ni by Ti in $LaNiO_3$ perovskites: A parameter governing the oxy-carbon dioxide reforming of methane. *Int. J. Hydrogen Energy* **2018**, *43*, 4136–4142. [CrossRef]
9. Haynes, D.J.; Campos, A.; Berry, D.A.; Shekhawat, D.; Roy, A.; Spivey, J.J. Catalytic partial oxidation of a diesel surrogate fuel using an Ru-substituted pyrochlore. *Catal. Today* **2010**, *155*, 84–91. [CrossRef]
10. Haynes, D.J.; Berry, D.A.; Shekhawat, D.; Spivey, J.J. Catalytic partial oxidation of n-tetradecane using Rh and Sr substituted pyrochlores: Effects of sulfur. *Catal. Today* **2009**, *145*, 121–126. [CrossRef]
11. Yan, L.; Hongjian, L.; Lipeng, Q.; Zhijin, W.; Linhai, W.; Yun-Quan, L. Improving anti-coking and sulfur-resisting performance of Rh-based lanthanum zirconate pyrochlore catalysts for diesel reforming through partial substitution with alkali earth metals. *J. Anal. Appl. Pyrolysis* **2023**, *169*, 105865.
12. Ma, Y.; Ma, Y.; Zhao, Z.; Ma, S.; Meng, Q.; Hu, X.; Buckley, C.E.; Dong, D. Fibrous $La_2Zr_2O_7$ pyrochlore-supported Ni nanocatalysts for methane reforming. *J. Phys. Chem. Solids* **2020**, *147*, 109643. [CrossRef]
13. Le Saché, E.; Pastor-Pérez, L.; Garcilaso, V.; Watson, D.J.; Centeno, M.A.; Odriozola, J.A.; Reina, T.R. Flexible syngas production using a $La_2Zr_{2-x}Ni_xO_{7-\delta}$ pyrochlore-double perovskite catalyst: Towards a direct route for gas phase CO_2 recycling. *Catal. Today* **2020**, *357*, 583–589. [CrossRef]
14. Kumar, N.; Kanitkar, S.; Wang, Z.; Haynes, D.; Shekhawat, D.; Spivey, J.J. Dry reforming of methane with isotopic gas mixture over Ni-based pyrochlore catalyst. *Int. J. Hydrogen Energy* **2019**, *44*, 4167–4176. [CrossRef]
15. Kumar, N.; Roy, A.; Wang, Z.; L'Abbate, E.M.; Haynes, D.; Shekhawat, D.; Spivey, J.J. Bi-reforming of methane on Ni-based pyrochlore catalyst. *Appl. Catal. A Gen.* **2016**, *517*, 211–216. [CrossRef]

16. Ashcroft, A.T.; Cheetham, A.K.; Foord, J.A.; Green ML, H.; Grey, C.P. Selective oxidation of methane to synthesis gas using transition metal catalysts. *Nature* **1990**, *344*, 319–321. [CrossRef]
17. Ashcroft, A.T.; Cheetham, A.K.; Green, M. Partial oxidation of methane to synthesis gas using carbon dioxide. *Nature* **1991**, *352*, 225–226. [CrossRef]
18. Ashcroft, A.T.; Cheetham, A.K.; Jones, R.H.; Natarajan, S.; Thomas, J.M.; Waller, D.; Clark, S.M. An in situ, energy-dispersive X-ray diffraction study of natural gas conversion by carbon dioxide reforming. *J. Phys. Chem.* **1993**, *97*, 3355–3358. [CrossRef]
19. Bespalko, N.; Roger, A.C.; Bussi, J. Comparative study of NiLaZr and CoLaZr catalysts for hydrogen production by ethanol steam reforming: Effect of CO_2 injection to the gas reactants. Evidence of Rh role as a promoter. *Appl. Catal. A Gen.* **2011**, *407*, 204–210. [CrossRef]
20. Bussi, J.; Musso, M.; Veiga, S.; Bespalko, N.; Faccio, R.; Roger, A.C. Ethanol steam reforming over NiLaZr and NiCuLaZr mixed metal oxide catalysts. *Catal. Today* **2013**, *213*, 42–49. [CrossRef]
21. Gaur, S.; Haynes, D.J.; Spivey, J.J. Rh, Ni, and Ca substituted pyrochlore catalysts for dry reforming of methane. *Appl. Catal. A Gen.* **2011**, *403*, 142–151. [CrossRef]
22. Sagar, T.V.; Sreelatha, N.; Hanmant, G.; Surendar, M.; Lingaiah, N.; Rama Rao, K.S.; Reddy, I.K.A.; Prasad, P.S. Influence of method of preparation on the activity of La–Ni–Ce mixed oxide catalysts for dry reforming of methane. *Rsc Adv.* **2014**, *4*, 50226–50232. [CrossRef]
23. Sagar, T.V.; Sreelatha, N.; Hanmant, G.; Upendar, K.; Lingaiah, N.; Rama Rao, K.S.; Reddy, I.K.A.; Prasad, P.S. Methane reforming with carbon dioxide over La-Ni_x-Ce_{1-x} mixed oxide catalysts. *Indian J. Chem.-Sect. A* **2014**, *53A*, 478–483.
24. Chen, H.S.; Kumar, R.V.; Glowacki, B.A. Chemical solution deposited lanthanum zirconium oxide thin films: Synthesis and chemistry. *Mater. Chem. Phys.* **2010**, *122*, 305–310. [CrossRef]
25. Koteswara Rao, K.; Banu, T.; Vithal, M.; Swamy GY, S.K.; Kumar, K.R. Preparation and characterization of bulk and nano particles of $La_2Zr_2O_7$ and $Nd_2Zr_2O_7$ by sol–gel method. *Mater. Lett.* **2002**, *54*, 205–210. [CrossRef]
26. Tong, Y.; Zhu, J.; Lu, L.; Wang, X.; Yang, X.J. Preparation and characterization of $Ln_2Zr_2O_7$ (Ln = La and Nd) nanocrystals and their photocatalytic properties. *J. Alloys Compd.* **2008**, *465*, 280–284. [CrossRef]
27. Bussi, J.; Bespalko, N.; Veiga, S.; Amaya, A.; Faccio, R.; Abello, M.C. The preparation and properties of Ni–La–Zr catalysts for the steam reforming of ethanol. *Catal. Commun.* **2008**, *10*, 33–38. [CrossRef]
28. Lima, S.M.; Assaf, J.M.; Pena, M.A.; Fierro, J.L.G. Structural features of $La_{1-x}Ce_xNiO_3$ mixed oxides and performance for the dry reforming of methane. *Appl. Catal. A Gen.* **2006**, *311*, 94–104. [CrossRef]
29. Xu, Z.; He, L.; Zhao, Y.; Mu, R.; He, S.; Cao, X. Composition, structure evolution and cyclic oxidation behavior of $La_2(Zr_{0.7}Ce_{0.3})_2O_7$ EB-PVD TBCs. *J. Alloys Compd.* **2010**, *491*, 729–736. [CrossRef]
30. Carley, A.F.; Jackson, S.D.; O'Shea, J.N.; Roberts, M.W. Oxidation states at alkali-metal-doped Ni (110)–O surfaces. *Phys. Chem. Chem. Phys.* **2001**, *3*, 274–281. [CrossRef]
31. Duan, Y.; Sun, F.; Yang, Y.; Chen, P.; Yang, D.; Duan, Y.; Wang, X. Thin-film barrier performance of zirconium oxide using the low-temperature atomic layer deposition method. *ACS Appl. Mater. Interfaces* **2014**, *6*, 3799–3804. [CrossRef]
32. Sagar, T.V.; Zavašnik, J.; Finšgar, M.; Novak Tušar, N.; Pintar, A. Evaluation of Au/ZrO_2 Catalysts Prepared via Postsynthesis Methods in CO_2 Hydrogenation to Methanol. *Catalysts* **2022**, *12*, 218. [CrossRef]
33. Kumar, P.; Shah, A.K.; Lee, J.H.; Park, Y.H.; Štangar, U.L. Selective hydrogenolysis of glycerol over bifunctional copper–magnesium-supported catalysts for propanediol synthesis. *Ind. Eng. Chem. Res.* **2020**, *59*, 6506–6516. [CrossRef]
34. Guan, D.; Ryu, G.; Hu, Z.; Zhou, J.; Dong, C.L.; Huang, Y.C.; Zhang, K.; Zhong, Y.; Komarek, A.C.; Zhu, M.; et al. Utilizing ion leaching effects for achieving high oxygen-evolving performance on hybrid nanocomposite with self-optimized behaviors. *Nat. Commun.* **2020**, *11*, 3376. [CrossRef]
35. Bachiller-Baeza, B.; Mateos-Pedrero, C.; Soria, M.A.; Guerrero-Ruiz, A.; Rodemerck, U.; Rodríguez-Ramos, I. Transient studies of low-temperature dry reforming of methane over Ni-CaO/ZrO_2-La_2O_3. *Appl. Catal. B Environ.* **2013**, *129*, 450–459. [CrossRef]

Disclaimer/Publisher's Note: The statements, opinions and data contained in all publications are solely those of the individual author(s) and contributor(s) and not of MDPI and/or the editor(s). MDPI and/or the editor(s) disclaim responsibility for any injury to people or property resulting from any ideas, methods, instructions or products referred to in the content.